

Mineralogical and textural evolution of the economic manganese mineralisation in western Rhodope massif, N. Greece

M. K. NIMFOPOULOS* AND R. A. D. PATTRICK

Department of Geology, The University, Manchester M13 9PL

Abstract

The western Rhodope massif contains a significant number of 'battery grade' Mn-oxide deposits which are best developed in the area near Kato Nevrokopi, Drama district, N. Greece. Economic Mn-oxide ore concentrations are confined to fault zones and related karsts in marbles. The mineralisation has formed by weathering of hydrothermal veins that were genetically related to Oligocene magmatism.

At Kato Nevrokopi, progressive and continuous weathering of primary, hydrothermal veins of rhodochrosite, mixed sulphide, quartz and 'black calcite' (calcite and todorokite) has resulted in the formation of the assemblage MnO-gel-(amorphous Mn-oxide)-todorokite-azurite-goethite-cerussite in the veins and the assemblage MnO-gel-nsutite-chalcophanite-birnessite-cryptomelane-pyrolusite and malachite and amorphous Fe-oxides in karstic cavities.

The f_{S_2} and f_{O_2} of the hydrothermal fluids increased with time. The breakdown of the hypogene Mn-carbonate was aided by the production of an acidic fluid due to the oxidation of sulphides. Precipitation of the supergene ores was caused by neutralisation of the fluids due to reaction with the host marble and to mixing of relatively reduced fluids with oxygenated surface water in a fluctuation water table regime. Zinc was also mobile during weathering and became concentrated in the intermediate Mn-oxides, effectively stabilising their structures. The mineral paragenesis records the progressive oxidation of the ore and the appearance of less hydrated Mn-oxides, low in alkalis and alkaline earths.

KEYWORDS: manganese oxides, supergene oxidation, Rhodope massif, Greece.

Introduction

THE western Rhodope massif hosts a large number of metallic mineral occurrences (Mn, Fe, Au, Ag, Pb, Zn, Cu) (Marinos, 1982) spatially and genetically related to Tertiary magmatism (Nimfopoulos, 1988; Nimfopoulos *et al.*, 1989) (Fig. 1). Exploitation of these mineral localities, especially for gold, dates back to ancient Macedonian times (300 B.C.) and continues today for manganese near Kato Nevrokopi, Drama, where mining of battery grade Mn-dioxide is in operation (4.5 million tons minimum total concentrate of Mn-dioxide produced so far).

Existing literature is limited to brief descriptions of the geology (Papastamatiou, 1952; Vacondios, 1982) and the mineralogy (Spathi, 1964; Podufal; 1971) of the deposits. This paper gives a detailed description of the mineralogy,

mineral chemistry, textures, and parageneses of the mineralising cycles at Kato Nevrokopi.

The mineralisation is hosted by a thick sequence of Palaeozoic marbles (the Upper Carbonate Sequence) which has been thrust over a sequence of alternating gneisses, mica schists, amphibolites and marbles (the Lower Gneiss Sequence) (Zachos and Dimadis, 1983). These sequences form the Rhodope Massif basement, which underwent lower amphibolite grade metamorphism between the Cambrian and Carboniferous (Maratos and Andronopoulos, 1964). Alpine deformation is represented by small-scale isoclinal folds and related northeast and northwest trending, steeply dipping, faults of Cretaceous to Oligocene age (Jordan, 1969).

The mineralisation at Kato Nevrokopi is confined to the intersections of the northeast and northwest trending faults and to the thrust zone forming the junction between the Upper Carbonate and the Lower Gneissic unit (Fig. 1). The

* Present address: IGME, Xanthi Branch, 30 Brocoumi Road, Xanthi 671 00, Greece.

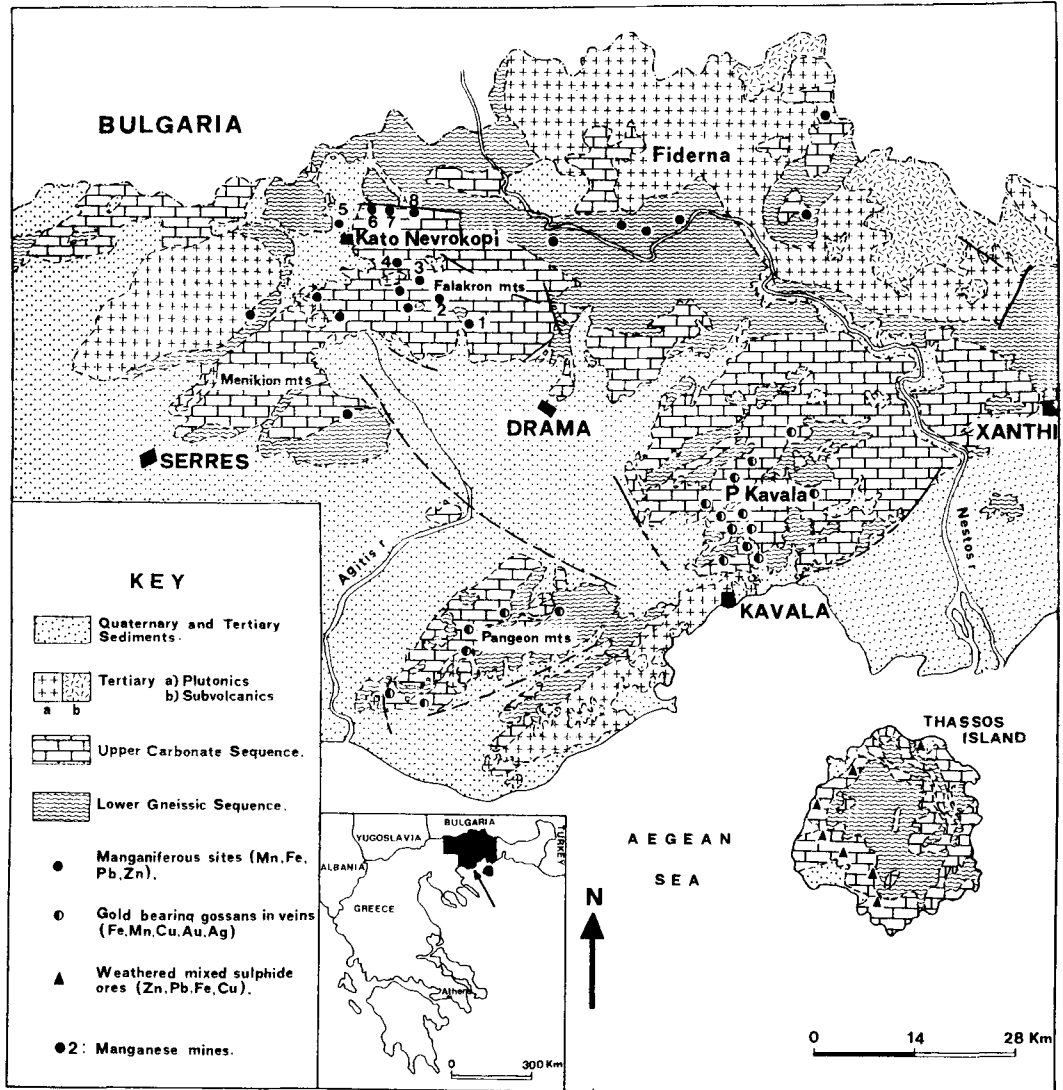


FIG. 1. Geology (redrawn from Dimadis and Zachos, 1986) and mineralisation of the western Rhodope massif. Manganese mines: 1, Pyrgi; 2, 25th km and Mavro Xylo; 3, Staren, Lagos and 28th km; 4, Granitis; 5, Synthia; 6, Karposluk; 7, Aghii Theodori; and 8, Tartana.

richest orebodies are found where the mineralisation has extended laterally into the marble. Negligible mineralisation occurs in the schist.

The shape of the primary orebodies is irregular with individual overshoots being lenticular or tubular, sub-parallel to the bedding, up to 50 m in length, 20 m in width and 5–10 m in thickness. Secondary Mn-oxide orebodies have the shape of the karstic cavities (dolines or sinkholes, up to 100 m in diameter, and 30 m depth).

On the basis of their setting and mineralogy, the ore zones can be divided into three categories: (a) The Deeper mineralised sulphide-carbonate-rich zones which at the time of the primary mineralisation were situated at significant depth and are exposed only in deeply eroded areas such as Pyrgi (Fig. 1).

(b) The Upper mineralised Mn-oxide-rich zones which at the time of the primary mineralisation were located near the surface (25th km, Mavro

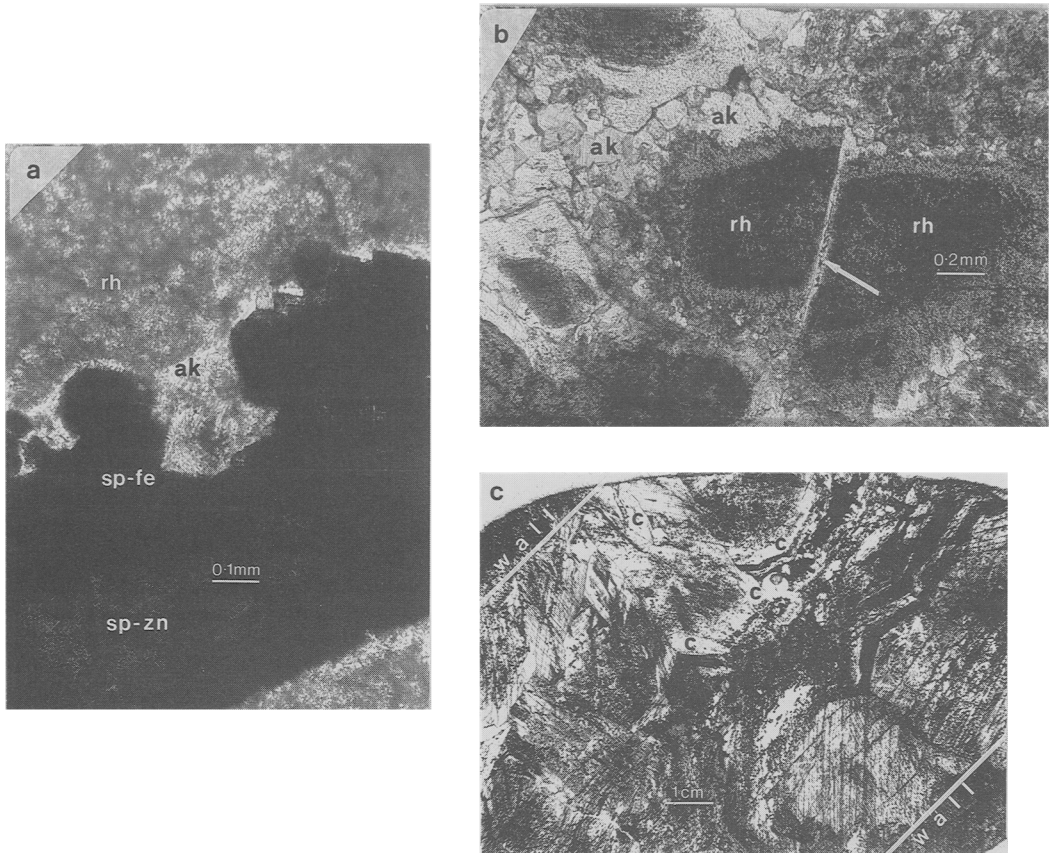


Fig. 2. Hypogene mineral texture micrographs at Pyrgi (PPL, transmitted): (a) Zoned sphalerite (sp-zn to sp-fe) is replaced by rhodochrosite (rh) and this in turn by ankerite (ak). There is sericite between sphalerite and rhodochrosite (near ak). (b) Zoned rhodochrosite (rh) is replaced by finely crystalline ankerite (ak) (indicated by an arrow) in a quartz vein hosted by marble. (c) Coarse calcite (c) perpendicular to the vein walls (marked in white) is lined by fine todorokite (black) in a black calcite vein.

Xylo, Staren, Lagos, 28th km, Granitis, Synthia, Karposluk, Aghii Theodori and Tartana mines). These zones are exposed in the higher altitude regions of the Falakron mountains.

(c) Secondary Mn-oxide in karstic cavities. In most mining areas the weathering products of the primary mineralisation were concentrated in karsts. These karstic orebodies have developed mainly from the Upper zone type mineralisation and therefore types (b) and (c) are found together.

Analytical methods

The study of the manganese mineral assemblages near Kato Nevrokopi is particularly difficult because of: (a) poor crystallinity, (b) intimate mixing of minerals, (c) poor polishing due to high

porosity, (d) the presence of Mn^{2+} , Mn^{3+} and Mn^{4+} in the same mineral, and (e) the lack of stoichiometry in the Mn-oxides and their variable H_2 content. Mineral identification therefore required detailed reflected light microscopy, X-ray diffraction (XRD) (Fig. 4) and electronprobe microanalysis (EPMA).

The hypogene mineralogy

The paragenesis of the hypogene ores has been determined using evidence from vein mineralisation throughout the region, although the best developed sulphide-rich mineralisation is at Pyrgi (Fig. 1). Quartz precipitation took place throughout the mineralising episode although it largely formed early in the sequence. Pyrrhotine was the first sulphide to form and, in association with the

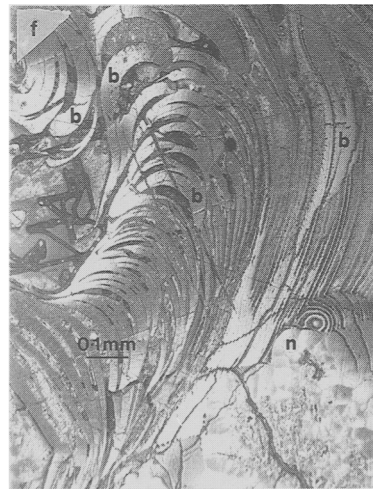
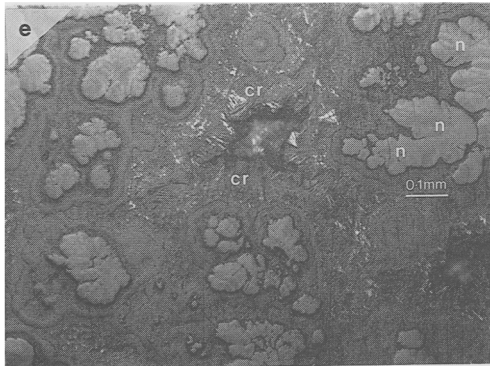
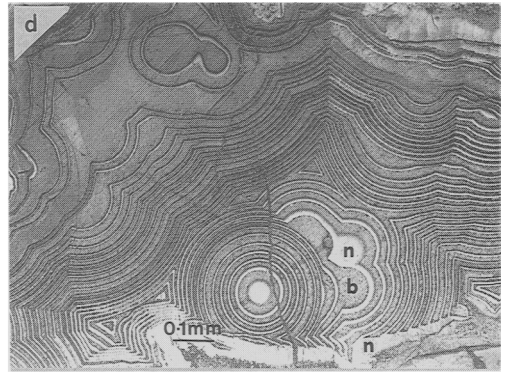
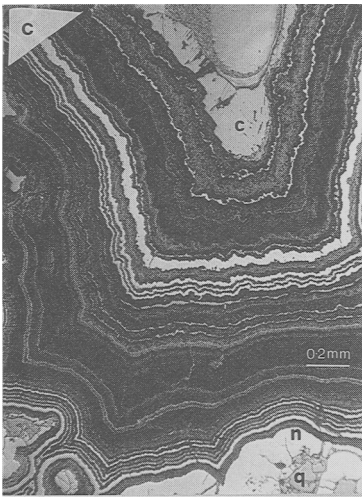
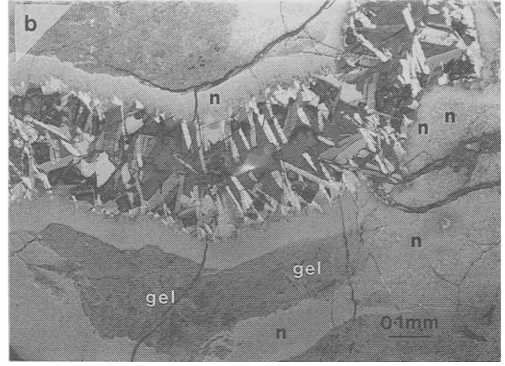
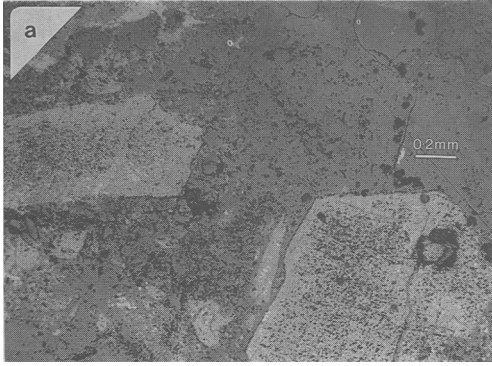


Table 1. EPMA of todorokite from Karposluk black calcite (wt.%).

No	MnO ₂	Fe ₂ O ₃	CaO	SiO ₂	MgO	Na ₂ O	K ₂ O	SrO	H ₂ O*
1	70.95	0.56	7.33	0.32	1.23	0.16	0.27	0.02	19.16
2	71.63	0.58	8.44	0.32	1.31	0.14	0.24	-	17.34
3	69.54	0.51	7.72	0.25	1.29	0.14	0.25	0.06	20.24
4	71.95	-	7.94	0.36	1.24	0.13	0.26	0.02	18.10
5	69.35	0.70	8.34	0.20	0.84	0.11	0.25	-	20.21
6	70.09	0.55	8.16	0.00	0.84	0.12	0.27	-	19.97
7	75.00	0.59	8.01	0.34	1.30	0.14	0.25	0.08	14.29
8	74.40	0.58	7.80	0.23	1.31	0.14	0.24	0.05	15.25
9	70.08	0.48	9.42	0.17	0.72	0.11	0.24	0.07	18.71

Table 2. Analyses of todorokite pseudomorphs after rhodochrosite in weathered veins at Mavro Xylo (wt.%).

No	MnO ₂	Fe ₂ O ₃	CaO	SiO ₂	MgO	K ₂ O	H ₂ O*
1	78.98	-	3.65	0.31	1.68	1.12	14.26
2	78.71	1.53	3.69	0.66	1.97	1.08	12.36
3	78.68	-	3.82	0.49	1.78	1.08	14.15
4	79.18	-	4.02	0.49	1.88	1.10	13.33
5	77.95	-	4.87	0.34	1.87	1.04	13.93
6	77.64	-	4.11	0.30	1.91	1.07	14.97
7	80.04	-	3.67	0.53	2.23	1.13	12.40
8	79.31	1.04	3.81	0.45	2.03	1.10	12.26
9	77.41	0.66	3.62	0.41	1.99	1.17	14.74

H₂O* : Estimated by difference assuming 100 wt.% total.

- : Not detected.

Wavelength peak-seeking revealed no detectable As, Ag, Mo and Ba.

quartz, replaced the carbonate host rocks. Pyrite occurs as euhedral grains (0.5–2 mm) in later rhodochrosite and replaces the pyrrhotine, such that only 3–5 µm blebs remain as inclusions in the pyrite. Sphalerite forms coarse, optically zoned grains (1 cm) and replaces quartz, pyrite and the host carbonate (Fig. 2a). Galena is common in the Upper zones where it occurs as altered aggregates with mixed Mn-oxides and, where present, in Deeper zones it replaces pyrite. Rare marcasite is

found replacing pyrite; and chalcopryrite replaces the other vein sulphides.

Rhodochrosite was the most abundant hypogene mineral in the lower zones but is now preserved only in the less weathered veins where it is present as rhombic and zoned acicular crystals (Fig. 2b) often replacing sphalerite (Fig. 2a). The rhodochrosite is brecciated and replaced by finely laminated ankerite, which is also present in vugs.

The last mineral to precipitate was vuggy

Fig. 3. Supergene mineral texture micrographs (reflected light). (a) Finely crystalline strongly birefractant pseudomorphs of todorokite (light grey to white) after rhodochrosite in a quartz vein hosted by the marble. Plane polarised light (PPL). (b) MnO-gel is veined and replaced by fine nsutite (n). Nsutite in turn is replaced by chalcophanite (grey to white, twinned) veinlets. Partially crossed polars (PCP). (c) A thick band of nsutite (n), including some detrital quartz (q), is overgrown by alternating layers of nsutite and amorphous Mn-oxides (light and dark grey) and eventually by coarse calcite (c). PPL. (d) Concentric bands of fine nsutite (n) and birnessite (b) in a cavity from a weathered vein. A shrinkage crack runs across both minerals. PPL. (e) Fine dendritic nsutite (n) surrounded by amorphous Mn⁺⁺-oxides of birnessitic composition (EPMA evidence) which, in turn, are replaced by fibrous, strongly anisotropic cryptomelane (cr) in vugs and cavities. PCP. (f) Veinlet of coarse pyrolusite, forming at the expense of fine pyrolusite material. PCP.

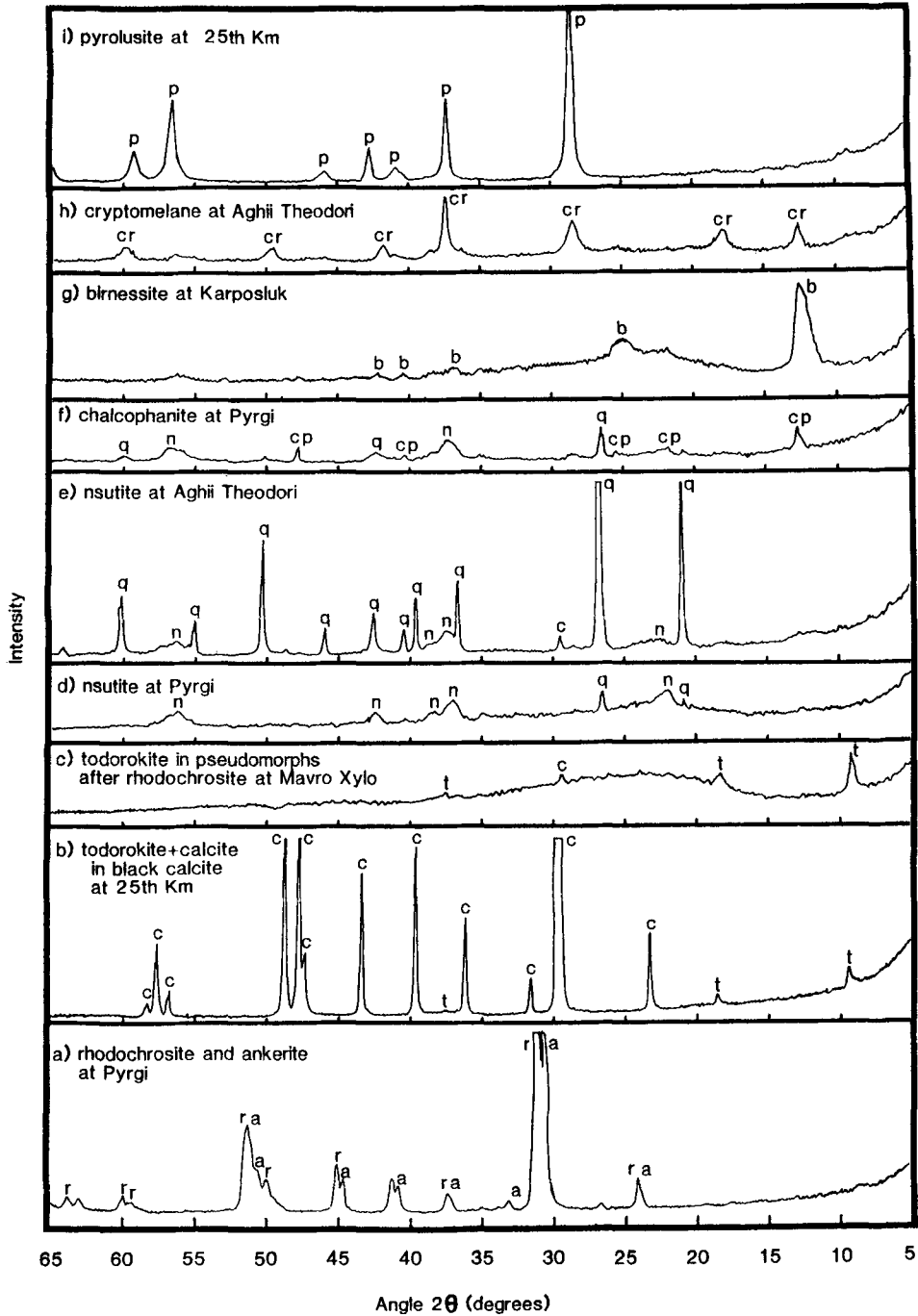


FIG. 4. Representative XRD diagrams of the Mn-minerals near Kato Nevrokopi. Cu-K α radiation with a curved graphite crystal monochromator was used. *r*, rhodochrosite; *a*, ankerite; *t*, todorokite; *c*, calcite; *n*, nsutite; *cp*, chalcophanite; *q*, quartz; *b*, birnessite; *cr*, cryptomelane; and *p*, pyrolusite.

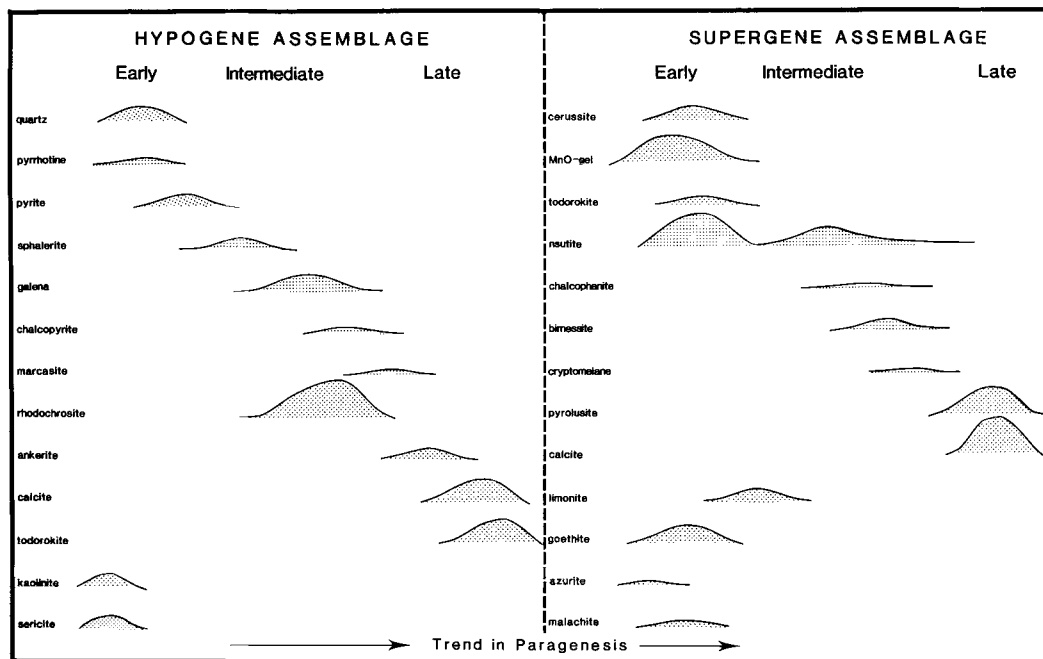


FIG. 5. Paragenetic sequence of the mineral assemblages found at Kato Nevrokopi. The peaks represent the percent amount of the total mineral precipitate at a given time.

calcite. In the Upper zones (25th Km, Karposluk and Tartana) the manganese is concentrated in 'black calcite' which comprises coarsely crystalline calcite intergrown and replaced by todorokite along cleavages (Fig. 2c).

Mineralogical zoning is expressed by the predominance of a quartz + rhodochrosite + sulphides assemblage in the deeper veins (e.g. Pyrgi) which is succeeded upwards by rhodochrosite + ankerite while near the surface veins of black calcite and galena predominate. Limited alteration adjacent to the veins has involved the processes of kaolinisation, sericitisation and dolomitisation.

Supergene mineralogy

The supergene mineralogy has developed by the progressive oxidation of the hypogene minerals, especially rhodochrosite. Two main processes operated: (a) the direct oxidation of rhodochrosite *in situ* to form amorphous and microcrystalline phases; (b) the dissolution of Mn^{2+} and precipitation in karstic cavities as Mn^{4+} -oxides.

In situ oxidation. The first breakdown product of rhodochrosite was 'MnO-gel', which contains predominantly Mn^{2+} . It forms as amorphous masses pseudomorphing rhodochrosite and is preserved in the veins just above the unaltered

sulphide-rich zones. In the more weathered veins (eg. Mavro Xylo, Karposluk) it is the Mn^{4+} -oxide, todorokite that replaces rhodochrosite (Fig. 3a), often forming prismatic pseudomorphs. Sulphide oxidation had resulted in the formation of azurite (chalcocopyrite), goethite (pyrite) and cerussite (galena).

Karst mineralisation. In the karst-hosted mineralisation found at relatively low altitudes nsutite is the most abundant Mn^{4+} -oxide. It forms microcrystalline aggregates (10–20 μm across) replacing MnO-gel (Fig. 3b). The nsutite is, in turn, replaced by chalcophanite (Fig. 3b), becoming less crystalline and eventually amorphous in contact with the chalcophanite. The strongly anisotropic platy crystals of chalcophanite have grown perpendicular to the vein walls and represent localised reaction of nsutite with Zn-rich fluids (Fig. 3b).

In the karsts developed at higher altitudes, MnO-gel is largely replaced by other Mn oxides. Although nsutite replaces the marbles it is mainly present as 0.2–1 cm layers and crusts containing detrital quartz and alternate layers of amorphous Mn-oxides (Fig. 3c). In the most weathered zones the nsutite is interlayered with birnessite (Fig. 3d) which also forms stripe-like aggregates lining cavities (Fig. 3f). Cryptomelane occurs in two samples (from Aghii and Theodori) where it

Table 3. Chemical composition of Mn-oxides in weathered veins and karstic cavities of low altitude (c.f. Pyrgi locality) (wt.%)

No	1	2	3	4	5	6	7	8	9	10	11	12	13	14	
		MNO-GEL			NSUTITE										CHALCOPHANITE
MnO ₂	70.08	67.56	70.35	70.24	86.89	85.79	85.19	86.66	87.87	85.01	88.57	73.29	74.89	76.35	
MnO									0.89	0.80	0.79				
Fe ₂ O ₃	2.83	3.28	0.91	0.82											
FeO	0.86	0.94	0.85	0.72	0.83	0.75	1.09	0.70	0.84	0.76	0.83		0.27	0.26	
SiO ₂	-	0.67	0.49	0.47	0.20	0.41	2.24	0.33	0.28	0.39	0.32	0.23	0.22	0.34	
ZnO	3.19	3.05	2.98	2.54	3.91	2.93	3.67	3.25	3.71	3.17	3.11	19.15	18.18	20.34	
MgO	0.04	0.01	0.02	0.03	0.03	0.01								0.02	
Na ₂ O	0.29	0.19	0.25	0.15	0.23	0.35	0.33	0.21	0.38	0.44	0.40	0.80	0.67	0.72	
K ₂ O	0.19	0.13	0.14	0.12	0.38	1.81	1.77	2.33	1.88	2.34	2.25	0.10	0.12	0.08	
SrO	0.23	0.05	0.09	0.11	0.04	0.13	0.09	0.05	0.01	0.08	0.05	0.01			
PbO	0.44	1.46	1.38	1.27	1.35	2.17	2.15	1.94	2.63	1.82	2.09				
H ₂ O*	21.85	22.66	22.54	23.53	6.14	5.65	3.47	3.64	1.60	5.39	1.59	6.42	5.65	1.89	

H₂O* :Determined by difference assuming total 100 wt.%. The analyses are from different grains in single samples.

- :Not detected.

Mn, Fe, Ca, Si and Zn were analysed by EDS and Mg, Na, K and Pb by WDS. Sr was analysed by both methods.

Analyses 1 to 4 are amorphous MnO-gel (Fig. 3b). Analyses 5 to 7 are nsutite veining the amorphous MnO-gel. Analyses 8 to 11 are nsutite replacing the marble wallrock. Analyses 12 to 14 are chalcophanite replacing nsutite (Fig. 3b).

Table 4. Chemical composition of Mn-oxides in higher altitude karsts (wt.%)

No	1	2	3	4	5	6	7	8	9	10	11	12	13	14
		NSUTITE			BIRNESSITE				CRYPTO MELAN	PYROLUSITE				
MnO ₂	94.02	91.37	92.35	92.54	78.73	76.62	70.92	68.63	65.64	94.88	96.00	96.28	96.14	96.69
ZnO	2.18	2.50	2.33	2.45	5.25	5.05	12.77	12.34	9.42	1.28	0.99	0.89		
CaO	0.71	0.93	0.93	0.84	2.09	2.02	3.31	3.12	2.27	0.56	0.63	0.64	0.48	0.54
Na ₂ O	0.09	0.14	0.11	0.12	0.32	0.30	0.53	0.51	0.40	0.05	0.06	0.05		
SiO ₂	0.10	0.11	0.13	0.11	0.08	0.08	0.03	0.03	0.09	0.57	0.68	0.59	0.69	0.56
K ₂ O	0.02	0.03	0.03	0.04	0.16	0.18	0.30	0.27	0.30					
BaO	0.64	0.70	0.71	0.70	2.07	1.96	1.73	1.74	0.12					
MgO									0.32					
As ₂ O ₅									2.68					
Al ₂ O ₃									1.45	0.04	0.03	0.08		
H ₂ O*	2.24	4.22	3.41	3.20	11.30	13.79	10.41	13.36	17.49	2.62	1.61	1.47	2.69	2.21

H₂O* :Determined by difference assuming total 100 wt.%. The analyses are from different grains in single samples.

- :Not detected.

Mn, Zn, Ca, As and Al were analysed by EDS and Na, Si, K and Ba by WDS. Mg was analysed by both methods.

Analyses 1 to 4 are nsutite and 5 to 6 birnessite at Karposluk (Fig. 3d) and 7 and 8 are birnessite deposited in cavities (Fig. 3f). Analyses 10 and 12 are pyrolusite at Karposluk and 13 to 14 are pyrolusite from Mavro Xylo.

forms fibrous aggregates (Fig. 3e) growing on the Mn-oxides. Pyrolusite also occurs in areas of advanced weathering, replacing nsutite. The progressive oxidation of pyrite is recorded by the sequence: goethite-amorphous iron oxide-limonite.

The full paragenesis and chemical evolution of the Kato Nevrokopi mineralisation are shown in Figs. 5 and 6.

Electron-probe microanalysis

Hypogene minerals. Analyses of rhodochrosite revealed the isostructural substitution of Mn, Ca and Mg, with CaO contents of up to 8.11 wt.% and MgO of 1.39 wt.%. The margins of the sphalerite grains are relatively enriched in iron (10.75 wt.%) compared to the rims (c. 5.75 wt.%), confirming the optical observations, and indicating the a_{FeS} increased during precipitation of the sphalerite. Despite the abundant todorokite in the black calcite veins, EPMA revealed the calcite to contain no detectable manganese. The Ca content of the todorokite (Table 1), however, is higher than previously recorded (Roy, 1981); the large Ca cations can be accommodated in the mineral's tunnel structure (Burns *et al.*, 1983).

Supergene mineral stoichiometry. The lack of stoichiometry and structure, the high cation exchange capacities, the low but variable Mn^{2+}

ratio of the Mn^{4+} -oxides, and their unanalysed H_2O -content (Ostwald, 1985, 1986) impose severe limitations on any accurate calculation of their formulae (Giovannoli and Brutsch, 1979). Average formulae are given for the Mn-oxides at Kato Nevrokopi and, except for MnO-gel which is considered to be a Mn^{2+} -oxide, the Mn is assumed to be tetravalent (Mn^{4+}).

Supergene vein minerals. The first formed amorphous MnO-gel approximates to the formula $(\text{Mn}^{2+}_{10.85}\text{Zn}_{0.40}\text{Ca}_{0.17}\text{Fe}^{2+}_{0.30}\text{Pb}_{0.06}\text{Si}_{0.08}\text{Na}_{0.08}\text{K}_{0.04}\text{Sr}_{0.01})\text{O}_{12} \cdot 13.92\text{H}_2\text{O}$ (Fig. 3b; Table 3) while the todorokite in pseudomorphs after rhodochrosite has a composition of $(\text{Ca}_{0.43}\text{Mg}_{0.29}\text{K}_{0.14}\text{Si}_{0.04}) \cdot (\text{Mn}^{4+}_{5.53}\text{Fe}^{3+}_{0.03})\text{O}_{12} \cdot 4.6\text{H}_2\text{O}$ (Fig. 3a; Table 2), revealing a distinctly lower Ca-content compared with the todorokite deposited in the 'black calcite' veins by hydrothermal fluids (Table 1).

Low altitude karsts. Veins of nsutite (Table 3) which replace hexagonal pseudomorphs of amorphous MnO-gel (Fig. 3b) contain distinctly higher potassium than the host mineral; later formed nsutite, $(\text{Mn}^{4+}_{5.66}\text{Zn}_{0.23}\text{Pb}_{0.05}\text{Fe}^{3+}_{0.05}\text{Ca}_{0.08}\text{K}_{0.26}\text{Na}_{0.07}\text{Si}_{0.03})\text{O}_{12} \cdot 0.96\text{H}_2\text{O}$, replacing the marble is generally less hydrated.

Chalcophanite $(\text{Zn}_{0.83}\text{Mn}^{4+}_{3.04}\text{Na}_{0.08}\text{Si}_{0.02}\text{Ca}_{0.01})\text{O}_7 \cdot 0.91\text{H}_2\text{O}$ (Table 3), is depleted in Ca and K compared to the nsutite it replaces; a

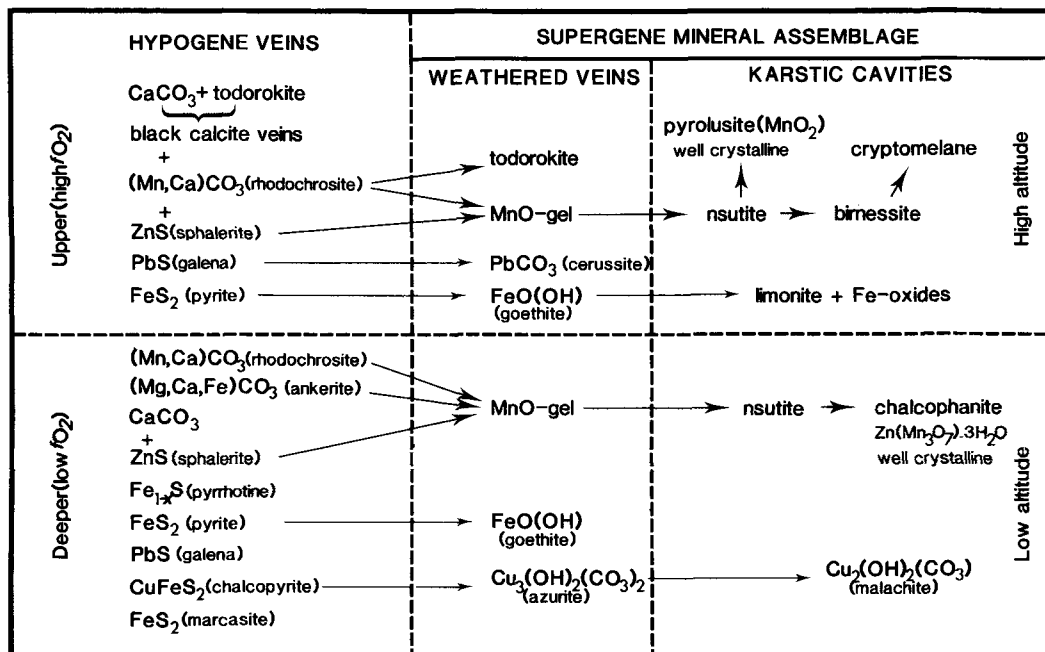


FIG. 6. Detailed presentation of the evolution of the supergene mineral assemblage found near Kato Nevrokopi.

consequence of their high mobility during weathering (Roy, 1981).

High altitude karsts. Nsutite was found to have a composition of $(\text{Mn}^{4+}_{5.86}\text{Zn}_{0.16}\text{Ca}_{0.08}\text{Ba}_{0.02}\text{Na}_{0.01}\text{Si}_{0.01})\text{O}_{12}\cdot\text{H}_2\text{O}$ (Table 4) at variance with the stoichiometry of $[\text{Mn}^{4+}_{1-x}\text{Mn}^{2+}_x]\text{O}_{2-2x}\cdot(\text{OH})_{2x}$ (where $x = 0.06\text{--}0.07$) suggested by Zwicker *et al.* (1962). Zinc substitutes for Mn^{2+} (Ortlepp, 1964) whereas Ca and Ba are located within the tunnel structures (Turner and Buseck, 1983).

Birnessite also contains some Zn as well as significant Ca, Ba, Na and K (Table 4). Early birnessite in concentric bands with nsutite (Fig. 3d) has a composition of $(\text{Mn}^{4+}_{6.56}\text{Zn}_{0.47}\text{Ca}_{0.27}\text{Ba}_{0.10}\text{Na}_{0.06}\text{K}_{0.02})\text{O}_{14}\cdot 5.1\text{H}_2\text{O}$ while the paragenetically late stripe-like aggregates of finely crystalline birnessite is more enriched in Zn: $(\text{Mn}^{4+}_{6.11}\text{Zn}_{1.18}\text{Ca}_{0.44}\text{Ba}_{0.09}\text{Na}_{0.09}\text{K}_{0.03})\text{O}_{14}\cdot 5\text{H}_2\text{O}$. These stripe-like aggregates show better crystallinity, a result of the increasing substitution of Mn by Zn, and increasing Ca and alkali-content (Giovannoli and Brutsch, 1979).

Analyses of cryptomelane from Aghii Theodori (Table 4) $[(\text{Mn}^{4+}_{6.75}\text{Zn}_{1.04}\text{Ca}_{0.36}\text{As}_{0.21}\text{Al}_{0.25}\text{Na}_{0.12}\text{Mg}_{0.07}\text{K}_{0.06}\text{Si}_{0.01}\text{Ba}_{0.01})\text{O}_{16}\cdot 8.7\text{H}_2\text{O}]$ indicate enrichment in Zn, As and Al, but depletion in K, compared with most published data of cryptomelane (Faulring *et al.*, 1960; Hewett and Olivares, 1968; Perseil and Pinet, 1976; Fransolet, 1979). Although cryptomelane is generally considered to be a K-bearing Mn-oxide, potassium is not essential to the structure. Indeed, there are cryptomelanes with even lower K-content (c. 0.09 wt.% K_2O ; Roy, 1981) than the one at Kato Nevrokopi, and Dubois (1936; cited by Roy, 1981) prepared the synthetic K-free phase $\alpha\text{-MnO}_2$, which showed an XRD pattern identical with that of cryptomelane.

Pyrolusite $[(\text{Mn}^{4+}_{5.90}\text{Zn}_{0.04}\text{Ca}_{0.05}\text{Si}_{0.05})\text{O}_{12}\cdot 0.63\text{H}_2\text{O}]$ analyses (Table 4) from the 25th km and Karposluk reveal it to be hydrated. The coarsely crystalline pyrolusite which formed at the expense of fine grained pyrolusite (Fig. 3f), has a lower H_2O , Ca and Mg content compared with its precursor phase, again a result of progressive weathering.

Discussion

The replacement textures of rhodochrosite (and sulphides) and the calcite around the veins, and the presence of kaolinite and sericite, give evidence of the reaction of the fluids with the marble wallrock. This would have resulted in a pH increase and was probably the principal mechanism for mineral precipitation (cf. Ander-

son, 1975). The large amounts of quartz (*T*-dependent solubility) in the veins also indicate a drop in the temperature of hydrothermal fluids (Fournier, 1985).

The replacement of pyrrhotine by pyrite (Brimhall, 1980) and the presence of marcasite in the veins (Gronvold and Westrum, 1976) indicate an increase in the sulphur fugacity of the hydrothermal fluids with time.

The presence of black calcite only in the upper zones indicates an increase in the oxidation state of the fluids with height in the veins. Hewett (1964) demonstrated that black calcite veins are typically found in a hot spring environment. Therefore, the black calcite veins could be interpreted as forming just below the discharge point of hot springs, in a zone of mixing with overlying oxygenated meteoric water.

The supergene mineralisation occurs in zones above the present level of a highly fluctuating water table. It is clear from the textures that manganese as Mn^{2+} was highly mobile during weathering processes and has been selectively leached from the hypogene veins and concentrated at different levels of the adjacent karsts. The present siting of karstic mineralisation above the water table is probably a combination of erosion and the fact that the water table was higher in the recent past, for instance during the ice age. The pseudomorphs after marble suggest that neutralisation of the fluids was one reason for precipitation. The encrustations and layers also indicate that Mn-bearing groundwaters were periodically flushed through the veins and karsts. As manganese (Mn^{2+}) solubility is much higher under reducing conditions, precipitation was probably caused by mixing of relatively acid, reduced, metal-bearing meteoric fluids that had reacted with the hypogene minerals with unmodified, oxygenated groundwater.

The presence of zinc in the supergene manganese minerals indicates the high mobility of the metal following the breakdown of sphalerite (Mann and Deutscher, 1980). The substitution of zinc can stabilise the non-stoichiometric, disordered Mn-oxides (Turner and Buseck, 1983). Substitution of vacant Mn^{4+} sites in the tunnel structure walls takes place by the mechanism $\text{Mn}^{4+} + \text{vacancy} = 2 \text{Zn}^{2+}$ with incorporation of the zinc atoms above and below the vacancy site (Burns *et al.*, 1983).

The manganese minerals show a general trend to phases with lower H_2O , alkali and alkaline earth contents. This is the result of a decrease in the size of the tunnel structures in the minerals formed. In minerals such as todorokite the large tunnels can accommodate water molecules and

alkalis. These are also susceptible to leaching during weathering and as the last-formed mineral, pyrolusite, has a small tunnel size, it contains little water, alkalis and alkaline earths (cf. Turner and Buseck, 1981).

Summary

The manganese mineralisation at Kato Nevrokopi is an example of a hypogene vein system that has undergone supergene enrichment to ore grade during weathering. The mineralogical evolution records the progressive oxidation of the ores with the development of a complex paragenetic sequence, dominated by the formation of Mn⁴⁺ oxides.

Acknowledgements

This project was funded by a 3 year Ph.D. research grant from the State Scholarships Foundation of Greece, for which our appreciation is recorded. We are indebted to Drs D. A. Polya, and G. T. R. Droop for fruitful discussions, two anonymous referees for critically reading the manuscript and to Elbomin for permission to access the mines. We would like to thank D. A. Plant and T. C. Hopkins for help with the EPMA, Emeritus Professor W. S. MacKenzie for providing the black calcite photograph, and Mrs T. Zioga for the preparation of a diagram.

References

- Anderson, G. M. (1975) Precipitation of Mississippi Valley-type ores. *Econ. Geol.*, **70**, 937–42.
- Brimhall, G. H., Jr. (1980) Deep hypogene oxidation of porphyry copper potassium-silicate protore at Butte, Montana: a theoretical evaluation of the copper remobilization hypothesis. *Ibid.*, **75**, 384–409.
- Burns, R. G., Burns, V. M., and Stockman, H. W. (1983) A review of the todorokite–buserite problem: implications to the mineralogy of marine manganese nodules. *Am. Mineral.*, **68**, 927–80.
- Dimadis, E. and Zachos, S. (1986) Geological map of Rhodope massif (1:200000). Unpubl., I.G.M.E., Xanthi.
- Faulring, G. M., Zwicker, W. K., and Forgong, W. D. (1960) Thermal transformations and properties of cryptomelane. *Am. Mineral.*, **45**, 946–59.
- Fournier, R. O. (1985) The behaviour of silica in hydrothermal solutions. In *Geology and Geochemistry of Epithermal Systems* (Berger, B. R., and Bethke, P. M., eds) Reviews in Econ. Geol. 2, 45–61.
- Fransolet, A. M. (1979) Occurrences of lithiophorite, nsutite and cryptomelane in Stavelot massif, Belgium. *Annal. Soc. Geol. Belg.*, **102**, 303–12.
- Giovanoli, R. and Brutsch, R. (1979) Über oxidhydroxide des Mn (IV) mit schichtgengitter, 5 Mitteilung: Stöchiometrie ausverhalten und die rolle bei der bildung von tiefsee-mangankonkretionen. *Chimia*, **33**, 372–76.
- Gronvold, F. and Westrum, E. F. Jr. (1976) Heat capacities of iron disulphides, thermodynamics of marcasite from 5–700K, pyrite from 350–770K, and the transformation of marcasite to pyrite. *J. Chem. Therm.*, **8**, 1039–48.
- Hewett, D. F. (1964) Veins of hypogene manganese oxide minerals in the South-Western United States. *Econ. Geol.*, **59**, 1429–72.
- and Olivares, R. S. (1968) High-potassium cryptomelane from Tarapaca province, Chile. *Am. Mineral.*, **53**, 1551–7.
- Jordan, H. (1969) Geology and petrography of the Bos-Dag area (Drama, Greek-Macedonia). *Geotekt. Forsch.*, **31**, 50–85.
- Mann, A. W. and Deutscher, R. L. (1980) Solution geochemistry of lead and zinc in water containing carbonate, sulphate, and chloride ions. *Chem. Geol.*, **29**, 293–311.
- Maratos, G. and Andronopoulos, B. (1964) Contribution to the geochronology of the crystalline schist of the Rhodope massif. *Bull. Geol. Soc. Greece*, **6**, 26–31.
- Marinos, G. (1982) Greece In *Mineral Deposits of Europe*, Volume 2 (Dunning, E. W., Mykura, W., and Slater, D., eds) IMM London, 233–53.
- Nimfopoulos, M. K. (1988) *Manganese mineralisation near Kato Nevrokopi, Drama, Greece*. Ph.D. thesis, University of Manchester, U.K., 259pp.
- Rex, D., and Patrick, R. A. D. (1989) Age of hydrothermal manganese mineralization near to Kato Nevrokopi, Drama, northern Greece. *Trans. Inst. Min. Met.*, **97**(B), 193–5.
- Ortlepp, R. J. (1964) Nsutite (battery grade manganese dioxide) from the Western Transvaal. *Trans. Geol. Soc. S. Africa*, **67**, 149–61.
- Ostwald, J. (1985) Some observations on the chemical composition of chalcophanite. *Mineral. Mag.*, **49**, 752–5.
- (1986) Some observations on the chemical composition of todorokite. *Ibid.*, **50**, 336–40.
- Papastamatiou, I. (1952) Ore mineralogical studies on the manganese deposits of the Drama area. *I.G.M.E.*, **274**, 28pp (in Greek).
- Perseil, E. A. and Pinet, M. (1976) Contribution a la connaissance des romanechites et des cryptomelanes-coronadites-hollandites. Traits essential et paragenesis. *Contrib. Mineral. Petrol.*, **55**, 191–204.
- Podufal, P. (1971) Zur geologie und lagerstattenkunde der manganvorkommen bei Drama (Griechisch-Makedonien) clauthaler. *Geol. Abh.*, **10**, 82pp.
- Roy, S. (1981) *Manganese deposits*. 458pp. Academic Press, London.
- Spathi, C. (1964) *The mineralogical composition of the Greek manganese ores*. Ph.D. thesis, University of Thessaloniki (in Greek with English abstract).
- Turner, S. and Buseck, P. R. (1981) Todorokites: a new family of naturally occurring manganese oxides. *Science*, **212**, 1024–27.
- (1983) Defects in nsutite (v-MnO₂) and dry cell battery efficiency. *Nature*, **304**, 143–46.

- Vacondios, I. (1982) *Preliminary geological and metallogenic study of Falakron region (Drama district)*. D.A. study, France, 43pp. (in French).
- Zachos, S. and Dimadis, E. (1983) The geotectonic position of the Skaloti-Echinos granite and its relation to the metamorphic formations of the Greek western and central Rhodope. *Geol. Balcan.*, **13**, 17–24.
- Zwicker, W. K., Meijer, W. O. J. G., and Jaffer, H. W. (1962). Nsutite—widespread manganese oxide mineral. *Am. Mineral.*, **47**, 246–66.

[Revised manuscript received 22 April 1991]